Calculating the frequencies and intensities of strongly anharmonic modes of adsorbates on surfaces: a low-cost but accurate computational approach

José A. Garrido Torres,[1,*] Jan P. Götze,[1] Federico Grillo,[1] Neville V. Richardson,[1] Herbert A. Früchtl,[1] Chris A. Hooley,[2] and Renald Schaub[1]

[1] *EaStCHEM and School of Chemistry, University of St Andrews, KY16 9ST, St Andrews, UK*
[2] *SUPA and School of Physics and Astronomy, University of St Andrews, KY16 9SS, St Andrews, UK*

(Dated: June 24, 2019)

We present a new method for calculating the frequencies and intensities of the vibrational modes of adsorbates on surfaces. Our method is based on density functional perturbation theory (DFPT) and provides accurate estimates of the vibrational intensities even when the vibrations are strongly anharmonic. Furthermore, it does so at a negligible additional computation cost compared to conventional DFPT calculation. We illustrate our method by calculating the vibrational spectra of three example systems — ethylidyne on Rh(111), benzene on Rh(111) coadsorbed with CO, and terephthalic acid (TPA) on Cu(100) — and comparing them to experimental measurements performed using High-Resolution Electron Energy Loss Spectroscopy (HREELS). We find excellent agreement between our predictions and the experimentally measured frequencies and intensities in all three cases.

Introduction. A common way of characterizing the nature and composition of functionalized surfaces is through the use of spectroscopic techniques. As vibrational features in the experimental signal are related to the electronic, molecular and atomic structure of the adsorbates, chemical sensitivity can be indirectly obtained by analyzing the features in the spectra. For instance, the use of Infrared (IR) and High-Resolution Electron Energy Loss Spectroscopy (HREELS) have helped to determine structural properties, such as adsorption sites[1], molecular orientation[2,3] or intermolecular arrangements[4–6] for a large variety of systems. These techniques also allow one to monitor the evolution of the adsorbed species due to changes in temperature and pressure conditions[7]. Monitoring these changes has been crucial for the detection of intermediate species which have ultimately helped to propose reaction mechanisms in heterogeneous catalysis[8–12].

Interpreting the experimental vibrational data, however, remains a significant challenge, and disentangling the origin of the signals can be non-trivial for spectra with a large number of vibrational features. As a consequence, a combination of experimental and theoretical vibrational information is usually necessary to obtain a comprehensive understanding of the system under study.

Density functional theory (DFT) is established as the method of choice for modeling interactions taking place in condensed matter systems and surfaces at the nanoscale level. Within the DFT framework, two numerical approaches have been commonly used to calculate vibrational frequencies and intensities.

The first approach relies on calculating the second-order derivative of the potential energy hypersurface with respect to the geometry (Hessian matrix) using finite differences within the harmonic approximation. Intensities are obtained by calculating the change in dipole moment for each vibration direction separately[13] which is computationally expensive and inefficient. Furthermore, this method can't guarantee a good description of the vibrational features since the magnitude of the displacements of the atoms are arbitrarily chosen.

The second approach involves calculating the Hessian matrix and Born effective charges of the system using density functional perturbation theory (DFPT) using the formula proposed by Giannozzi *et al.*[14] and Baroni *et al.*[15]. This method has proven to be computationally more efficient and has provided accurate theoretical descriptions of vibrational features of adsorbates at metal surfaces[16–19].

Despite the considerable success of this method, some of the computed features remain in disagreement with the experimental spectra. The most commonly encountered issue is the overestimation of some calculated intensities, which have been mainly attributed to anharmonic effects[16,20,21]. However, to date no strategy with an affordable computational cost has been suggested to overcome the discrepancy between theoretical and experimental vibrational features.

Here, we propose a novel approach to correcting vibrational frequencies and intensities using DFPT. We provide an analytic expression for the Morse potential which allows us to obtain anharmonic corrections for fundamental transitions using Born effective charges (BEC). This correction can be used to correct spectra for anharmonicities with almost negligible cost with respect to the DFPT calculations.

In the remainder of this article, we explain our method and use it to predict the vibrational frequencies and intensities for three example physical systems. We then present experimental measurements of these quantities, made via HREELS: in our own group in one case, and reproduced from the literature in two other. We obtain excellent agreement between the predicted and experimentally measured values in all cases. Finally, we discuss the wider application of our technique, including the importance of the density functional used in the calculation.

Theoretical method. The conventional calculation of HREELS intensities from the vibrational eigenmodes of molecules is based on the assumption that the oscillation

in each eigenmode is harmonic. If this is the case, then the eigenstates of the quantum harmonic oscillator can be used to calculate the dipole matrix element between the ground state and the excited state, and the square modulus of this matrix element gives the intensity.

In the case where the mode is strongly anharmonic, this procedure cannot be used. However, many anharmonic vibrations fit well to the Morse potential form,

$$V(x) = D\left(1 - e^{-a(x-r_e)}\right)^2, \tag{1}$$

where x is the displacement from equilibrium along the particular vibrational eigenmode in question, and D, a, and r_e are constants. We determine these constants from DFT calculations.

Armed with this Morse-potential fit for the anharmonic mode, we then transform the dipole operator into its representation in terms of the eigenmode coordinates, and thus calculate the dipole matrix element using the known formula[22] for the matrix element of the co-ordinate x between the ground and first excited states of the potential (1). This allows us to make a prediction of the HREELS intensity based on an accurate (albeit approximate) representation of the potential experienced by the molecule when it undergoes that mode of vibration. We emphasize that the additional computational cost of this approach compared to conventional harmonic predictions of HREELS intensities is negligible.

Our calculations were performed using periodic DFT employing a plane-wave basis set, using PAW (Projector Augmented Wave[23,24]) as implemented in VASP[25–28]. Valence electrons were described using plane-waves considering an expansion on the kinetic energy up to an energy cut-off of 400 eV. For the smearing of the electron population distribution we employed the first order Methfessel-Paxton method[29], using a smearing width of 0.1 eV. The convergence criterion for the electronic self-consistent cycle was fixed at 10^{-6} eV and the forces on all ions were required to be smaller than 0.015 eV/Å.

Structural optimizations were carried out using the optPBE-vdW functional[30], which intrinsically includes dispersion to account for vdW interactions. Standard PBE[31,32] calculations are included to highlight the importance of choosing the appropriate functional in order to obtain accurate spectra.

The Rh(111) and Cu(100) surfaces were modeled using a slab composed of four layers (with the two upper layers relaxed during optimizations). A vacuum of 15 Å was introduced in the direction orthogonal to the surface. The optimizations were carried out using 5×5×1 k-points for ethylidyne (2×2 coverage) and benzene/CO ($2\sqrt{3}$×4 coverage) on Rh(111). 3×3×1 k-points are used for TPA on Cu(100) (3×3 and 4×4 coverages).

The Hessian matrix and Born effective charges (BEC) of the previously optimized structures were calculated using DFPT as implemented in VASP. Vibrational intensities are calculated using linear response as proposed by D. Karhánek *et al.*[16] using the formula introduced by Giannozzi *et al.*[14] and Baroni *et al.*[15]:

$$I(\omega) = \sum_{i=1}^{3}\Big[\sum_{k=1}^{N}\sum_{j=1}^{3} Z_{ij}(k)\ e_j(k)\Big]^2, \tag{2}$$

where I(ω) is the intensity for the ω-th vibrational mode, N is the number of atoms and $i, j \in \{x, y, z\}$, label the directions in a Cartesian basis. $Z_{i,j}(k)$ corresponds to the BEC for the k-th atom when displaced in the direction j producing an effect in the polarization in the direction i. $e_i(k)$ is the eigenvector for the ω-th vibrational mode with displacement in the component i for the k-th atom.

One of the advantages of the HREELS technique is its capability to detect dipole (same selection rules as IR) and impact scattering (with a weak orientation dependence) modes. The possibility of recording signals originating from these two phenomena allows the access to information related to the molecular orientation. In order to consider this, the intensities of each mode are split in the three Cartesian coordinates as:

$$\begin{aligned} I(\omega) = a\Big[\sum_{k=1}^{N}\sum_{j=1}^{3} Z_{xj}(k)\ e_j(k)\Big]^2 \\ +b\Big[\sum_{k=1}^{N}\sum_{j=1}^{3} Z_{yj}(k)\ e_j(k)\Big]^2 + c\Big[\sum_{k=1}^{N}\sum_{j=1}^{3} Z_{zj}(k)\ e_j(k)\Big]^2, \end{aligned} \tag{3}$$

where the three components of the intensity can be weighted using the parameters a, b and c.

HREELS experiments show a decay of the intensity with increasing frequency[33]. This is implemented in our model as the following transfer function:

$$I_d(\omega) = \frac{I(\omega)}{\nu}, \tag{4}$$

where $I_d(\omega)$ is the corrected intensity for the decay of the ω-th mode and ν the frequency of that particular mode.

In order to obtain a correction factor for the previously obtained intensities using the harmonic approximation, the following theoretical procedure is followed.

The dipole intensity of a given transition can be expressed as

$$I = |M|^2, \tag{5}$$

where the matrix element M is given by

$$M = \langle \psi_f | \hat{O} | \psi_i \rangle\,. \tag{6}$$

Here $|\psi_i\rangle$ is the ground state of the molecule, $|\psi_f\rangle$ is the state with one quantum of energy in the eigenmode of interest and all other modes in their ground states, and the dipole operator is given by

$$\hat{O} = \sum_{k=1}^{N}\sum_{ij} E_i Z_{k,ij} \hat{r}_{k,j}. \tag{7}$$

In this equation, E_i is the component of the electric field in Cartesian direction $i, j \in \{x, y, z\}$, $Z_{k,ij}$ is a 3×3N matrix containing the Born effective charges for the k-th atom when displaced in the direction j producing an effect in the polarization in the direction i, and $\hat{r}_{k,j}$ is the operator for the j-component of the position of the k-th atom.

To evaluate the matrix element M, the $\hat{r}_{k,j}$ operator needs to be replaced by its expansion in terms of the normal-mode coordinates. This is done by inverting the set of normal-mode eigenvectors $\boldsymbol{e}_i$. To be specific, let the vector $\hat{\boldsymbol{r}}$ be the $3N$-component vector whose components are $\hat{x}_1$, $\hat{y}_1$, $\hat{z}_1$, $\hat{y}_2$, ..., where $\hat{x}_1$ is the operator for the x-coordinate of the first atom and so on. Then the operator for the coordinate of the i-th normal mode is given by

$$\hat{q}_i = \boldsymbol{e}_i \cdot \hat{\boldsymbol{r}}. \tag{8}$$

Making a vector of all the normal-mode coordinates, the following matrix equation is obtained:

$$\begin{pmatrix} \hat{q}_1 \\ \hat{q}_2 \\ \hat{q}_3 \\ \hat{q}_4 \\ \vdots \\ \hat{q}_{3N} \end{pmatrix} = \underbrace{\begin{pmatrix} \cdots & \boldsymbol{e}_1 & \cdots \\ \cdots & \boldsymbol{e}_2 & \cdots \\ \cdots & \boldsymbol{e}_3 & \cdots \\ \cdots & \boldsymbol{e}_4 & \cdots \\ \vdots & \vdots & \vdots \\ \cdots & \boldsymbol{e}_{3N} & \cdots \end{pmatrix}}_{\equiv A} \begin{pmatrix} \hat{x}_1 \\ \hat{y}_1 \\ \hat{z}_1 \\ \hat{x}_2 \\ \vdots \\ \hat{z}_N \end{pmatrix}.$$

Since we know the components of the $3N \times 3N$ matrix $\boldsymbol{A}$ explicitly, it is feasible to invert this matrix, to obtain, $\boldsymbol{A}^{-1}$ (the eigenvectors $\boldsymbol{e}_i$ require to be normalized before contracting the matrix A). Once the matrix $\boldsymbol{A}^{-1}$ is obtained, the construction of the Cartesian coordinate operators in terms of the normal mode ones is done via:

$$\begin{pmatrix} \hat{x}_1 \\ \hat{y}_1 \\ \hat{z}_1 \\ \hat{x}_2 \\ \vdots \\ \hat{z}_N \end{pmatrix} = \boldsymbol{A}^{-1} \begin{pmatrix} \hat{q}_1 \\ \hat{q}_2 \\ \hat{q}_3 \\ \hat{q}_4 \\ \vdots \\ \hat{q}_{3N} \end{pmatrix},$$

which can be written in component form,

$$\hat{r}_i = \sum_{j=1}^{N} [A^{-1}]_{ij} \hat{q}_j. \tag{9}$$

We can substitute this expression back into equation 7 to obtain the form of the dipole operator:

$$\hat{O} = \sum_{i=1}^{3}\sum_{j=1}^{3N} E_i \tilde{Z}_{ij} \hat{r}_j = \sum_{i=1}^{3}\sum_{j=1}^{3N} E_i \tilde{Z}_{ij} \sum_{k=1}^{3N} [\boldsymbol{A}^{-1}]_{jk} \hat{q}_k. \tag{10}$$

This can be simplified by defining the $3N$-component vector $\boldsymbol{s}$, whose components s_k are given by

$$s_k = \sum_{i=1}^{3}\sum_{j=1}^{3N} E_i \tilde{Z}_{ij} [\boldsymbol{A}^{-1}]_{jk}. \tag{11}$$

Therefore,

$$\hat{O} = \sum_{k=1}^{3N} s_k \hat{q}_k. \tag{12}$$

The matrix element M is given by

$$M = \langle \psi_f | \hat{O} | \psi_i \rangle = \sum_{k=1}^{3N} s_k \langle \psi_f | \hat{q}_k | \psi_i \rangle \tag{13}$$

The matrix element in the summand, $\langle \psi_f | \hat{q}_k | \psi_i \rangle$, will vanish for any k which is not the eigenmode of interest (i.e. the eigenmode that has one more quantum of energy in $|\psi_f\rangle$ than it does in $|\psi_i\rangle$). Let this eigenmode be labelled as j. The resulting matrix element M reduces to

$$M = s_j \langle 1 | \hat{q}_j | 0 \rangle \tag{14}$$

where $|0\rangle$ is the ground state and $|1\rangle$ is the first-excited state of the Morse potential oscillator. The matrix element $\langle 1 | \hat{q}_j | 0 \rangle$ is known[22]:

$$\langle 1 | \hat{q}_j | 0 \rangle = f \equiv \frac{2}{2N-1} \sqrt{\frac{N(N-1)\Gamma(2N)}{\Gamma(2N+1)}}, \tag{15}$$

where $|f|^2$ is the correction factor for the intensity of a given mode, $\Gamma(z)$ is the gamma function, and N is given by

$$N = \frac{\sqrt{2D}}{a} - \frac{1}{2}, \tag{16}$$

with D and a the parameters from the Morse potential for the eigenmode j. Note that the matrix element in equation 15 is unity in the harmonic case.

The intensity is corrected as:

$$I_{anh} = |f|^2 I, \tag{17}$$

where I_{anh} is the corrected intensity and I the intensity obtained using the harmonic approximation. Single-point energies (calculated using VASP) along the dimensionless coordinates of each mode are calculated on an equally spaced grid (10 single-points) to obtain the one-dimensional potential energy surface (1D-PES) of each mode. To ensure that the different modes are comparable, the mass-weighted normal coordinates (eigenvectors of the dynamical matrix) must be transformed into dimensionless coordinates as proposed by Gregurick *et al.*[34].

The 1D-PES obtained for each mode are fitted to a Morse potential (see equation 1).

The non-linear least squares algorithm is used to fit the curves, minimizing the coefficient of determination until R^2 >0.99 to ensure an accurate fit for each mode. The parameters obtained from the fit (D_e and a) for each mode are introduced in equation 16 to calculate the relative anharmonic correction factors.

Finally, the calculated spectra were broadened using a Gaussian profile with a full width half maximum (FWHM) corresponding to the instrumental resolution of the experiments. This is 50 cm^{-1} for the spectra of the two molecules (benzene and ethylidyne) adsorbed on Rh(111) and 60 cm^{-1} for TPA on Cu(100).

Experimental details. HREELS measurements for ethylidyne on Rh(111) were carried out operating the spectrometer in the specular geometry within a dedicated Ultra-High Vacuum (UHV) system. The system is composed of a preparation chamber with base pressure $< 5{\times}10^{-10}$ mbar and an analysis chamber with base pressure $< 1{\times}10^{-10}$ mbar. Ethene (C_2H_4, 99.995% purity) molecules were dosed at room temperature (300 K) for an exposure of 2 L, which ensures saturation coverage. The resolution of the spectra is 50 cm^{-1}. The presence of residual CO in the chamber was minimized by keeping on the vacuum gauges only for the time necessary to set the pressures for cleaning (Ar and O_2 treatments) and for the initial ethene dose. As a consequence, the spectra do not indicate features related to adsorbed CO.

The experimental spectra shown for ethylidyne on Rh(111) were collected in-house, the TPA on Cu(100) and mixed benzene/CO on Rh(111) systems are taken from Refs. 3 and 4, respectively. The spectrum for benzene/CO on Rh(111) is adapted with permission from B. E. Koel, J. E. Crowell, C. M. Mate and G. A. Somorjai, *J. Phys. Chem.*, 1984, **88**, 1988-1996. Copyright 1984 American Chemical Society. The spectrum for TPA on Cu(100) is adapted with permission from Y. Ge, H. Adler, A. Theertham, L. L. Kesmodel and S. L. Tait, *Langmuir*, 2010, **26**, 16325-16329. Copyright 2010 American Chemical Society.

Results and discussion. The ethylidyne (C_2H_3) radical is strongly adsorbed on Rh(111), forming a chemisorbed layer with a (2×2) structure at saturation coverage[35]. The most stable relaxed geometry in our calculations is in agreement with the experiments: the molecule is adsorbed on a three-fold hollow site with its C−C axis perpendicular to the surface[35].

The calculated geometry of the most stable configuration found at this coverage is in agreement with the experiments showing the C−C axis of the molecule perpendicular to the surface and centered above a three-fold hollow site[35]. The calculated spectra using the optimized geometry and the one obtained experimentally are shown in Figure 1a.

The calculated frequency values obtained with the harmonic approximation and after the anharmonic corrections are systematically close to the experimental values, with small discrepancies that are comprised between 6 and 35 cm^1. In contrast, the calculated intensities using the harmonic approximation exhibit large discrepancies with the experiments, with a high overestimation of the bands related to the stretching modes ν_{CC} (1075 cm^{-1}) and ν_{CH} (2095 cm^{-1}). The intensity of these bands decreases after applying the anharmonic corrections, resulting in an excellent agreement with the experimental relative intensities.

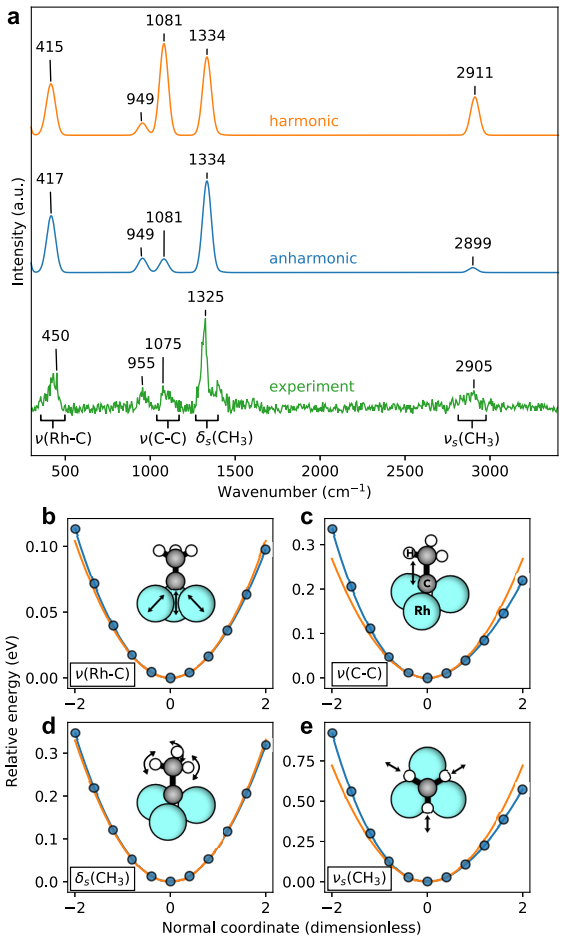

Figure 1. HREEL spectra for (2×2)-(C_2H_3) on Rh(111). (a) Calculated harmonic (in orange), harmonic including anharmonic corrections (in blue), and experimental (in green) spectra. Frequency values are included for the most relevant bands (in cm^{-1}). (b-e) Resulting energy evaluations (blue circles) for the scanned normal coordinates of the following fundamental vibrational modes of ethylidyne: (b) Rh−C stretching, (c) C−C stretching, (d) CH_3 wagging, and (e) C−H stretching. Morse fit is represented with solid blue lines. Harmonic potential curves for each mode (solid orange lines) are included to highlight the difference between the harmonic and anharmonic potentials (blue solid lines). Arrows in the models are set to graphically represent the motion of each vibrational mode.

For the second system in this study, we focus on the adsorption of benzene on Rh(111) in the presence of CO. Ordering of adsorbed benzene on this metal substrate is increased in the presence of coadsorbed CO, leading to the formation of a c(2$\sqrt{3}$×4)rect structure[4]. The most stable configuration found in our calculations is in agreement with the experimental data[4,36]. This structure contains one CO molecule per unit cell with benzene adsorbed on hollow sites. Benzene adopts a flat-lying geometry with its aromatic ring parallel to the surface. The benzene molecule is distorted from the D_{6h} geometry due

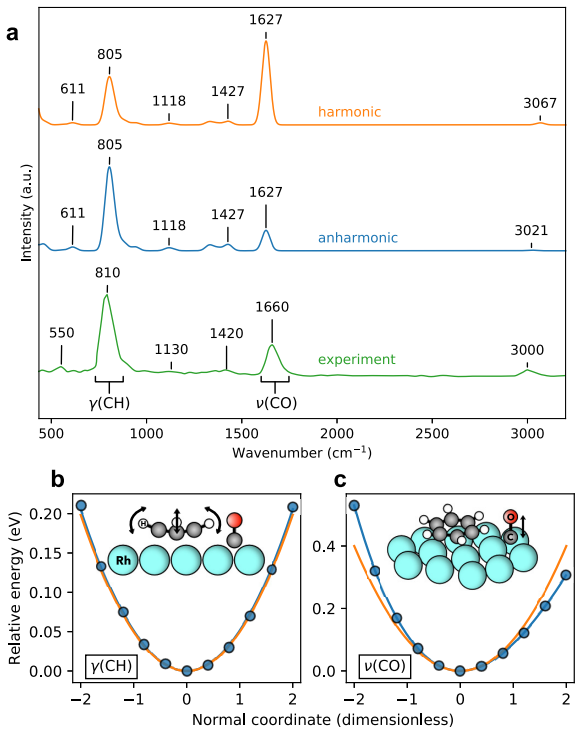

Figure 2. HREEL spectra for c(2$\sqrt{3}$×4)rect-C_6H_6/CO on Rh(111). (a) Calculated harmonic (in orange), harmonic including anharmonic corrections (in blue), and experimental (in green) spectra. Frequency values are included for the most relevant bands (in cm^{-1}). (b, c) Resulting energy evaluations (blue circles) for the scanned normal coordinates of the following fundamental vibrational modes of benzene: (b) CH_3 wagging and (c) C−O stretching. Harmonic potential curves for each mode (solid orange lines) are included to highlight the difference between the harmonic and anharmonic potentials (blue solid lines). Arrows in the models are set to graphically represent the motion of each vibrational mode. Experimental spectrum is adapted from Ref. 4.

to the strong metal-π interaction, which produces a tilting of the C−H bonds away from the surface. In this structure the CO molecule is adsorbed upright on a hollow site (see model in Figure 2).

The theoretical and experimental spectra for the c(2$\sqrt{3}$×4)rect-C_6H_6/CO on Rh(111) configuration are shown in Figure 2a. The most intense experimental bands are related to the C−H out-of-plane bending mode of benzene (γ_{CH}) at ∼810 cm^{-1} and the stretching of the CO (ν_{CO}) at ∼1660 cm^{-1}.

The bands at 550, 1130, 1420 and 3000 cm^{-1} are assigned to the Rh−C stretching ($\nu_{Rh-C_6H_6}$), CH scissoring (δ_{CH}), ring deformation due to the C−C stretching (ν_{CC}) and C−H stretching (ν_{CH}). The largest discrepancy for the frequency values between theory and experiments is found for the $\nu_{Rh-C_6H_6}$ mode (∼61 cm^{-1}). For the other modes the differences are comprised between 5 and 33 cm^{-1}. The calculated intensities using the harmonic approximation for the bands $\nu_{Rh-C_6H_6}$ at 611 cm^{-1}, γ_{CH} at 805 cm^{-1}, δ_{CH} at 1118 cm^{-1}, δ_{CC} at 1427 cm^{-1} and ν_{CH} at 3067 cm^{-1} are in excellent agreement with the experiments. However, the intensity of the CO peak (1627 cm^{-1}) is drastically overestimated.

After applying the anharmonic corrections, the band derived from the γ_{CH} mode becomes the most intense. Remarkably, this mode is essentially harmonic (see Figure 2b), thus, the changes in relative intensities when applying the anharmonic corrections can't be assigned to this mode. Indeed, this change comes from the correction of the highly anharmonic C−O stretching. The asymmetry in the bond length contraction (strong interatomic repulsion) and elongation produces a deviation from the harmonic potential for the ν_{CO} mode as show in Figure 2c) . The anharmonicity of this mode can even be more pronounced because the CO molecule is adsorbed upright and the electron density in the vacuum and substrate regions are expected to be very different.

Again, the anharmonic corrections improve considerably the relative intensities of the peaks. After these corrections the theoretical and experimental spectra are in much better agreement.

The last system case of study presented here is the adsorption of TPA ($C_6H_4(COOH)_2$) on Cu(100). TPA is adsorbed flat on this substrate at submonolayer coverage[3,37,38]. Upon heating up to 100°C, the two carboxylic groups deprotonate, forming islands with a square-commensurate (3×3) structure[37]. The adsorption geometry of TPA on Cu(100) when forming (3×3) structures has been reported before, experimentally[38] and theoretically[39]. The optimized structure in this work resembles those reported. The theoretical and experimental spectra corresponding to this structure are included in Figure 3a.

The two most intense experimental peaks are the C−H bend(γ_{CH}, at 752 cm^{-1}) and O−C−O bend (δ_{OCO}, at 879 cm^{-1}). The weak bands at 1104, 1307, 1342 and 1542 cm^{-1} are assigned to the C−H bend (δ_{CH}), C−C stretching (ν_{CC}), O−C−O symmetric ($\nu_{s(OCO)}$) and O−C−O asymmetric ($\nu_{a(OCO)}$) stretching, respectively. The very weak signal observed at 3032 cm^{-1} is attributed to the C−H stretching. The agreement between the calculated and observed frequency values is reasonably good. The calculated frequencies only differ by 48 (γ_{CH}) and 9 cm^{-1} (δ_{OCO}) with respect to the experiments. The largest frequency discrepancies are found for the symmetric ν_{CH} (81 cm^{-1}).

In general, there is a good agreement between the relative intensities of the calculated spectrum using the harmonic approximation and the experiments. However, the peak at 871 cm^{-1} seems to be overestimated even when applying anharmonic corrections. The scanned energies along the γ_{CH} mode (Figure 3b) indicate that anharmonicity is not the cause of the discrepancy in intensity between theory and experiment for this mode. Other effects, such as those originated by the intermolecular interaction due to coverage, must be taken into consideration. The mismatch between the calculated and experi-

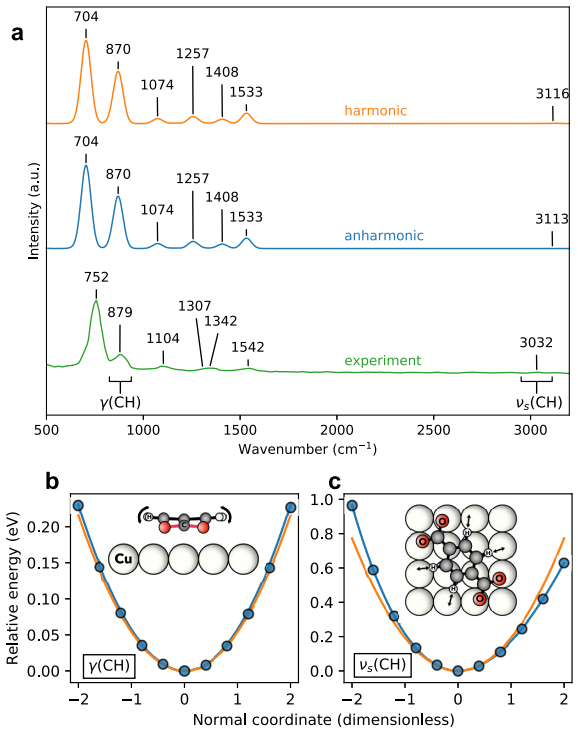

Figure 3. HREEL spectra for (3×3)-TPA on Cu(100). (a) Calculated harmonic (in orange), harmonic including anharmonic corrections (in blue), and experimental (in green) spectra. Frequency values are included for the most relevant bands (in cm^{-1}). (b, c) Resulting energy evaluations (blue circles) for the scanned normal coordinates of the following fundamental vibrational modes of TPA: (b) C−H (b) bend and (c) C−H symmetric stretching. Harmonic potential curves for each mode (solid orange lines) are included to highlight the difference between the harmonic and anharmonic potentials (blue solid lines). Arrows in the models are set to graphically represent the motion of each vibrational mode. Experimental spectrum is adapted from Ref. 3.

mental intensities of the γ_{CH} signal is reduced when considering simulating the spectra using a mixture of structures (see Supplemental Material).

The importance of the choice of functional is also reviewed in this work (see Supplemental Material). Our method was applied to simulate spectra for the three aforementioned systems employing two different functionals, PBE and optPBE-vdW. Conclusively, the spectra calculated using optPBE-vdW provide the best agreement with the experiments. The results obtained using PBE are similar to those obtained with optPBE-vdW for the two chemisorbed systems, ethylidyne on Rh(111) and benzene/CO on Rh(111). In contrast, this method fails dramatically in the description of the vibrations for the adsorption of TPA on Cu(100). This is expected since the GGA functionals are not usually the best choice to describe geometries and binding energy of systems involving aromatic molecules on coinage metals[40–43]. Therefore, we emphasize that the functional must be wisely chosen in order to obtain accurate vibrational information.

Summary. In this work we have shown that the use of anharmonic corrections is required for many solid state systems in order to obtain an accurate description of vibrational frequencies and intensities. We propose a novel approach for calculating HREEL spectra by explicitly taking into account anharmonic effects. In general, this method shows greatly improved performance for describing vibrational intensities of molecules adsorbed on metal surfaces. Remarkably, these corrections have only a small additional cost with respect to DFT calculations.

We have analyzed three systems to show the improvement in the quality of the calculated HREEL spectra due to these corrections: ethylidyne on Rh(111), benzene and CO coadsorbed on Rh(111) and TPA on Cu(100). The calculated vibrational features of the molecules adsorbed with flat-lying geometries, such as benzene or TPA, are usually well-described when using the harmonic approximation. However, the modes that are essentially perpendicular to the surface have very asymmetric potential energy curves, therefore they are not well-described using the harmonic approximation. This is the context in which our method has shown to be essential for calculating accurate intensities.

Acknowledgment: We acknowledge financial support from the Scottish Funding Council (through EaStCHEM and SRD-Grant HR07003) and from EPSRC (PhD studentship for JAGT, EP/M506631/1). Present address for JPG: Institut für Chemie und Biochemie, Freie Universität Berlin, 14195, Berlin, Germany. The research data supporting this publication can be accessed at https://doi.org/10.17630/4287c913-fbd6-4412-891f-9f2cf644c4c1[44]. The software package supporting this publication can be accessed at https://github.com/jagarridotorres/Vibtools[45].

* jagt@st-andrews.acu.uk

[1] T. Hayashi, Y. Morikawa, and H. Nozoye, J. Chem. Phys. **114**, 7615 (2001).
[2] J. Greenwood, H. A. Früchtl, and C. J. Baddeley, J. Phys. Chem. C **117**, 22874 (2013).
[3] Y. Ge, H. Adler, A. Theertham, L. L. Kesmodel, and S. L. Tait, Langmuir **26**, 16325 (2010).
[4] B. E. Koel, J. E. Crowell, C. M. Mate, and G. A. Somorjai, J. Phys. Chem. **88**, 1988 (1984).
[5] H. Ohtani, B. Bent, C. Mate, M. Van Hove, and G. Somorjai, Appl. Surf. Sci. **33-34**, 254 (1988).
[6] F. Grillo, J. A. Garrido Torres, M.-J. Treanor, C. R. Larrea, J. P. Götze, P. Lacovig, H. A. Früchtl, R. Schaub, and N. V. Richardson, Nanoscale **8**, 9167 (2016).
[7] W. Mao, J. H. He, Y. J. Xi, W. Chen, K. Wu, C. Zhang, E. S. Tok, and G. Q. Xu, J. Phys. Chem. C **120**, 24780

(2016).
[8] B. E. Bent, C. M. Mate, J. E. Crowell, B. E. Koel, and G. A. Somorjai, J. Phys. Chem. **91**, 1493 (1987).
[9] Q. Chen, T. Rada, A. McDowall, and N. V. Richardson, Chem. Mater. **14**, 743 (2002).
[10] M. Sock, A. Eichler, S. Surnev, J. Andersen, B. Klötzer, K. Hayek, M. Ramsey, and F. Netzer, Surf. Sci. **545**, 122 (2003).
[11] H. Zhang, Q. Fu, Y. Cui, D. Tan, and X. Bao, J. Phys. Chem. C **113**, 8296 (2009).
[12] B. Wang, M. König, C. J. Bromley, B. Yoon, M. J. Treanor, J. A. Garrido Torres, M. Caffio, F. Grillo, H. Früchtl, N. V. Richardson, F. Esch, U. Heiz, U. Landman, and R. Schaub, J. Phys. Chem. C **121**, 9413 (2017).
[13] D. Porezag and M. R. Pederson, Phys. Rev. B **54**, 7830 (1996).
[14] P. Giannozzi and S. Baroni, J. Chem. Phys. **100**, 8537 (1994).
[15] S. Baroni, S. De Gironcoli, A. Dal Corso, and P. Giannozzi, Reviews of Modern Physics **73**, 515 (2001).
[16] D. Karhánek, T. Bučko, and J. Hafner, J. Phys. Condens. Matter **22**, 265006 (2010).
[17] S.-S. Lee, B. Kim, and S. Lee, J. Phys. Chem. C **118**, 20840 (2014).
[18] M. Seydou, J. Teyssandier, N. Battaglini, G. T. Kenfack, P. Lang, F. Tielens, F. Maurel, and B. Diawara, RSC Adv. **4**, 25698 (2014).
[19] A. Davantès, D. Costa, and G. Lefèvre, J. Phys. Chem. C **119**, 12356 (2015).
[20] M. P. Andersson, J. Blomquist, and P. Uvdal, J. Chem. Phys. **123**, 224714 (2005).
[21] K. Forster-Tonigold, X. Stammer, C. Wöll, and A. Groß, Phys. Rev. Lett. **111**, 086102 (2013).
[22] J. A. C. Gallas, Phys. Rev. A **21**, 1829 (1980).
[23] P. E. Blöchl, Phys. Rev. B **50**, 17953 (1994).
[24] G. Kresse and D. Joubert, Phys. Rev. B **59**, 1758 (1999).
[25] G. Kresse and J. Furthmüller, Phys. Rev. B **54**, 11169 (1996).
[26] G. Kresse and J. Furthmüller, Comput. Mater. Sci. **6**, 15 (1996).
[27] G. Kresse and J. Hafner, Phys. Rev. B **49**, 14251 (1994).
[28] G. Kresse and J. Hafner, Phys. Rev. B **47**, 558 (1993).
[29] M. Methfessel and A. T. Paxton, Phys. Rev. B **40**, 3616 (1989).
[30] J. Klimeš, D. R. Bowler, and A. Michaelides, J. Phys. Condens. Matter **22**, 022201 (2010), arXiv:0910.0438.
[31] J. P. Perdew, K. Burke, and M. Ernzerhof, Phys. Rev. Lett. **77**, 3865 (1996).
[32] Y. Zhang and W. Yang, Phys. Rev. Lett. **80**, 890 (1998).
[33] H. Ibach and D. L. Mills, *Electron Energy Loss Spectroscopy and Surfaces Vibrations* (Academic Press, 1982).
[34] S. K. Gregurick, G. M. Chaban, and B. R. Gerber, J. Phys. Chem. A **106**, 8696 (2002).
[35] A. Wander, M. A. Van Hove, and G. A. Somorjai, Phys. Rev. Lett. **67**, 626 (1991).
[36] C. Mate, C.-T. Kao, and G. A. Somorjai, Surf. Sci. **206**, 145 (1988).
[37] S. L. Tait, Y. Wang, G. Costantini, N. Lin, A. Baraldi, F. Esch, L. Petaccia, S. Lizzit, and K. Kern, J. Am. Chem. Soc. **130**, 2108 (2008).
[38] S. L. Tait, H. Lim, A. Theertham, and P. Seidel, Phys. Chem. Chem. Phys. **14**, 8217 (2012).
[39] J. D. Fuhr, A. Carrera, N. Murillo-Quirós, L. J. Cristina, A. Cossaro, A. Verdini, L. Floreano, J. E. Gayone, and H. Ascolani, J. Phys. Chem. C **117**, 1287 (2013).
[40] J. Carrasco, W. Liu, A. Michaelides, and A. Tkatchenko, J. Chem. Phys. **140**, 084704 (2014).
[41] J. Klimeš, D. R. Bowler, and A. Michaelides, Phys. Rev. B **83**, 195131 (2011), arXiv:1102.1358.
[42] K. Toyoda, I. Hamada, S. Yanagisawa, and Y. Morikawa, J. Nanosci. Nanotechnol. **11**, 2836 (2011).
[43] J. Wellendorff, A. Kelkkanen, J. J. Mortensen, B. I. Lundqvist, and T. Bligaard, Top. Catal. **53**, 378 (2010).
[44] J. A. Garrido Torres, J. P. Götze, F. Grillo, N. V. Richardson, H. Früchtl, C. A. Hooley, and R. Schaub, Dataset. University of St Andrews Research Portal (2019), https://doi.org/10.17630/4287c913-fbd6-4412-891f-9f2cf644c4c1.
[45] J. A. Garrido Torres, J. P. Götze, F. Grillo, N. V. Richardson, H. Früchtl, C. A. Hooley, and R. Schaub, Vibtools. Software Package. University of St Andrews (2019), https://github.com/jagarridotorres/Vibtools.